ADVANCED MATERIALS
www.advmat.de

Multistage pH-Responsive Liposomes for Mitochondrial-Targeted Anticancer Drug Delivery

Ran Mo, Qiong Sun, Jingwei Xue, Nan Li, Wenyuan Li, Can Zhang, and Qineng Ping*

In recent years, a myriad of intravenously administrated nanoparticle (NP)-based drug delivery systems such as liposomes,[1] micelles,[2] and albumin nanoparticles[3] have been used for preclinical and clinical cancer therapy. The anticancer efficacy of NPs depends on their ability to reach the target sites of action. Delivery of NPs from the injection site to the final antitumor targets consists of various transport steps with multiple physiological and biological barriers, including transport via blood to the tumor extracellular matrix (organ level), binding to the cell membrane (tissue level), internalization (cellular level), and intracellular delivery (cellular level and subcellular level) in turn.

At the organ level from blood to tumor, although the enhanced permeability and retention (EPR) effect, used as passive targeting, plays an important role in accumulation and retention of NPs at the tumor site, the safety and stability in the blood resulting from the surface chemistry of NPs, such as surface charge, are basic prerequisites for NPs to have pharmaceutical applications. For intravenous administration, NPs with positive charge cause severe cytotoxicity, serum inhibition, rapid clearance from the plasma compartment, and instability with opsonin,[4] and thus cannot be used in vivo. However, at the tissue level, the positive charge of NPs facilitates their cellular uptake by means of binding through electrostatic interaction with negatively charged plasmalemma and subsequent internalization.[5] In an attempt to exploit the mildly acidic tumor microenvironment (pH 6.0–7.0)[6] to increase NP retention in tumors, much research has focused on NPs functionalized to change their surface charge from neutral/negative to positive when triggered by the tumor extracellular pH, for enhanced tumor cellular uptake.[7]

At the cellular level, the major internalization mechanism of NPs is clathrin-mediated endocytosis, in which NPs are mainly located in endosomes (pH 5.0–6.0) but also in lysosomes (pH 4.0–5.0). The endolysosomes are regarded as the overriding intracellular barrier to NP delivery, owing to the degradation of NPs and their cargo by endolysosomal acid and hydrolase. Accordingly, NPs responsive to endolysosomal pH have been formulated for endolysosomal escape and payload release. These designs include nanovectors with a) pH-cleavable linkers bonded to drugs;[8] b) pH-induced charge conversion;[9] c) pH-stimulant membrane fusion and disruption;[10] d) pH-triggered swelling;[11] and e) chemical agents for endosomal escape.[12] At the subcellular level, it is essential for a number of NPs liberated into the cytosol to deliver their encapsulated anticancer drugs to organelle targets for subcellular targeting, including nuclear and mitochondrial targeting. Mitochondrial targeting is a descriptor generally applied to enhance efficiency and specificity of anticancer drugs for cancer treatment,[13] since mitochondria, the powerhouses of the cells, are implicated in the regulation of cellular differentiation and growth as well as programmed cell death, especially in tumor cells.[14] Despite these extraordinary advances, the majority of previous reports have only paid attention to overcoming one or two barriers, such as charge conversion or endolysosomal escape. Hence, an easy-to-fabricate nanocarrier system that can vanquish successive physiological and biological barriers from blood to organelles for anticancer drug delivery is still lacking and remains highly desirable.

In the work reported here, we designed, synthesized, and evaluated a novel mitochondrial-targeted nanocarrier system based on zwitterionic oligopeptide liposomes ($HHG2C_{18}$-L) with multistage pH response to break down the series of barriers mentioned above in the whole-process delivery. $HHG2C_{18}$-L consists of soy phosphatidylcholine (SPC), cholesterol, and a synthetic smart lipid (1,5-dioctadecyl-L-glutamyl 2-histidyl-hexahydrobenzoic acid, $HHG2C_{18}$). $HHG2C_{18}$ carries two amino acid groups (glutamic acid and histidine) and one pH-cleavable group (hexahydrobenzoic amide) as a hydrophilic block, and two stearyl alkane chains as a hydrophobic block, which resembles natural phospholipids in the structure. The characteristic of $HHG2C_{18}$-L is the multistage pH response to the mildly acidic tumor microenvironment and the acidic intracellular compartment, successively (**Figure 1**). Typically, the surface charge of $HHG2C_{18}$-L under physiological conditions (pH 7.4), such as in blood, is strongly negative. As $HHG2C_{18}$-L arrive at the tumor site by means of the EPR effect, the initial-stage pH response occurs, in which the surface charge of $HHG2C_{18}$-L reverses to positive to increase tumor cellular uptake on account of electrostatic attraction to the negatively charged tumor cell membrane. Accompanied by endocytosis into the endosomes and lysosomes, the subsequent-stage pH response takes place, in which the imidazole group of histidine in $HHG2C_{18}$ facilitates proton influx (proton sponge effect) to endolysosomes, leading to endolysosomal bursting, and the hydrolysis of hexahydrobenzoic amide brings about a stronger positive surface charge of $HHG2C_{18}$-L by the loss of carboxy groups in $HHG2C_{18}$, hindering a charge reconversion from positive to negative when $HHG2C_{18}$-L escape from endolysosomes to the cytoplasm

Dr. R. Mo, Q. Sun, Dr. J. W. Xue, N. Li, Prof. C. Zhang, Prof. Q. N. Ping
Center of Drug Discovery
State Key Laboratory of Natural Medicines
China Pharmaceutical University
24 Tong Jia Xiang, Nanjing 210009, P. R. China
E-mail: zhangcan@cpu.edu.cn
W. Y. Li
Faculty of Pharmacy and Pharmaceutical Sciences
Monash University
381 Royal Parade, Parkville, VIC 3052, Australia

DOI: 10.1002/adma.201201498

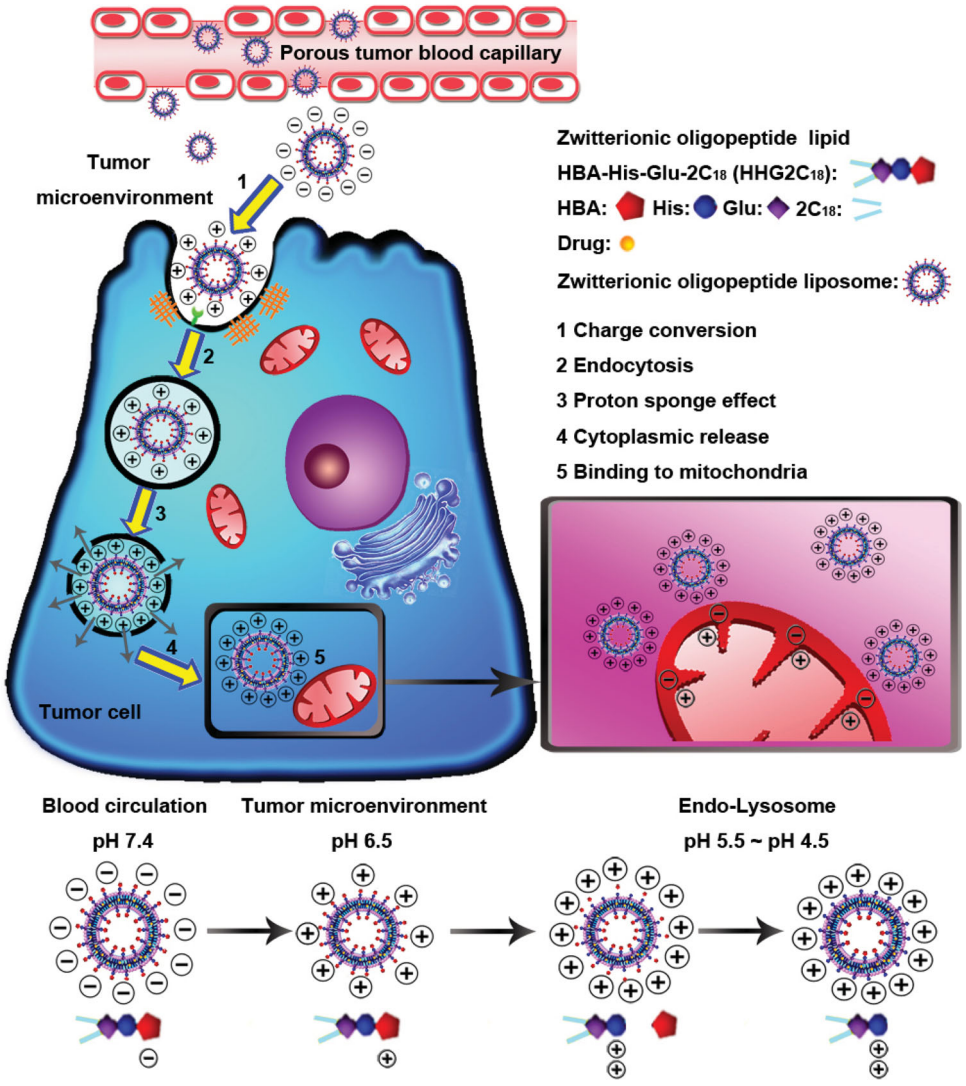

Figure 1. Schematic design of the smart liposomes ($HHG2C_{18}$-L) with multistage pH response to the tumor extracellular matrix and intracellular compartments for mitochondrial-targeted anticancer drug delivery.

(pH 7.2–8.0). Finally, $HHG2C_{18}$-L carrying a high positive charge have the ability to accumulate at the mitochondria by electrostatic interaction for mitochondrial targeting, owing to the transmembrane electric potential of mitochondria of up to approximately 130–150 mV (negative inside).[15] Therefore, the intelligent liposomes provide a safe and efficient carrier platform for cascade mitochondrial drug delivery on the basis of the kinetic process from blood to mitochondria.

For proof of our idea, we synthesized $HHG2C_{18}$ by ester linkage and amide linkage (Scheme S1, Supporting Information), and successfully prepared the bare and drug-loaded $HHG2C_{18}$-L and the conventional liposomes (SPC-L) as a control by the classic film dispersion method. Temsirolimus (CCI-779), a Food and Drug Administration (FDA)-approved drug against renal cancer, was encapsulated in the lipid bilayer of the liposomes. Hydrophobic coumarin 6 (C6) with non-specific mitochondrial targeting was chosen as a fluorescent probe with a similar loading location in the liposomes to CCI-779. The entrapment efficiencies of CCI-779 and C6 in $HHG2C_{18}$-L were approximately 96.75% and 93.76%, respectively, and the drug-loaded liposomes had a larger particle size than the bare liposomes (Figure S1a, Supporting Information). There was no significant difference in the particle size of $HHG2C_{18}$-L in the buffer solution at various pH values. The transmission electron microscopy (TEM) image confirmed the spherical shape of CCI-779-loaded $HHG2C_{18}$-L (CCI-779/$HHG2C_{18}$-L) (Figure S1b, Supporting Information).

To demonstrate the first-stage pH response of $HHG2C_{18}$-L to the tumor extracellular acidity, we measured the zeta potential of $HHG2C_{18}$-L dispersed in the buffer solutions at various pH values (pH 7.4, 6.5, 5.5, 4.5) (**Figure 2**a). The pH values of 7.4, 6.5, 5.5, and 4.5 simulated that of the physiological environment, tumor microenvironment, and endosomal and lysosomal compartments, respectively. The zeta potential of $HHG2C_{18}$-L changed sharply from negative (–22.9 mV) to positive (+6.3 mV) over the narrow pH range of 7.4–6.5, indicating that the neutral

Adv. Mater. **2012**,
DOI: 10.1002/adma.201201498

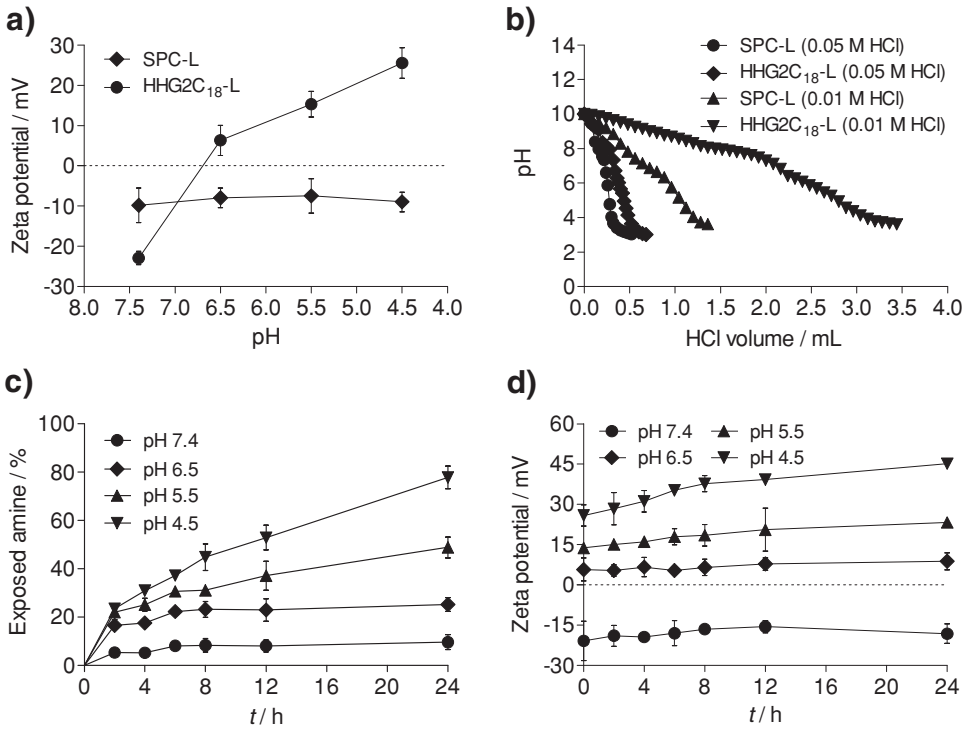

Figure 2. a) Zeta potential of $HHG2C_{18}$-L and SPC-L at different pH values. b) Acid titration profiles of aqueous solutions of $HHG2C_{18}$-L and SPC-L. Solutions of each liposome were adjusted to pH 10 using 0.3 M NaOH and then titrated with 0.05 M or 0.01 M HCl. c) Degradation of the hexahydrobenzoic amide in $HHG2C_{18}$-L at different pH values. d) Zeta potential variation of $HHG2C_{18}$-L accompanying the degradation of the hexahydrobenzoic amide at different pH values.

point of $HHG2C_{18}$-L was about pH 6.8, where the zeta potential became zero. Moreover, the increasing acidity had a concomitant increase in the positive charge of the $HHG2C_{18}$-L. The zeta potential of $HHG2C_{18}$-L continuously rose to +15.3 mV at pH 5.5 and +25.5 mV at pH 4.5. By contrast, the pH-non-responsive SPC-L showed a constant zeta potential at all pH values investigated. Accordingly, $HHG2C_{18}$-L had the ability to change the zeta potential according to the environmental pH, which was attributed to the chemical structure of the zwitterionic lipid, which includes the carboxy group of hexahydrobenzoic acid and the amino group of histidine. It was confirmed that charge conversion of $HHG2C_{18}$-L from negative to positive occurred in the mildly acidic tumor microenvironment, and endowed $HHG2C_{18}$-L with stronger positive charge at the endolysosomal acidities.

Generally, the effects of the highly positively charged NPs on endolysosomal escape are mainly defined as the proton sponge effect, by determining the buffering capacity, and membrane disruption, by evaluating hemolysis (the breakdown of red blood cells). $HHG2C_{18}$-L caused little hemolysis, regardless of the concentration or pH value (Figure S2, Supporting Information), whereas it showed a remarkable pH-buffering effect (proton sponge effect) for neutral to acidic conditions (Figure 2b). In other words, $HHG2C_{18}$-L containing histidine with an imidazole ring are able to absorb protons at endolysosomal pH as the second-stage pH response, leading to an increase in osmotic pressure inside the endolysosomes, followed by plasma membrane disruption and $HHG2C_{18}$-L release into the cytoplasm.

If the charge conversion of NPs is only dependent upon protonation/deprotonation of the amino and carboxyl groups, the NPs escaping from endolysosomes to the cytoplasm undergo surface charge reconversion from positive to negative, causing loss of interactions with the mitochondria. Acid-labile β-carboxylic acid amides present pH-dependent hydrolysis, in contrast to unsubstituted amides, as a result of nucleophilic catalysis by the carboxylic acid. The reaction proceeds via an addition intermediate, from which the amine is expelled, producing a cyclic anhydride as the second product.[16] The fluorescamine (4′-phenylspiro[2-benzofuran-3,2′-furan]-1,3′-dione) method, based on the reaction between the exposed primary amine of histidine and fluorescamine, was used to evaluate the pH-dependent hydrolysis of the hexahydrobenzoic amide. As shown in Figure 2c, the resulting amide in $HHG2C_{18}$-L exhibited great degradability at pH 5.5 and pH 4.5. When hydrolysis at pH 7.4 is taken as a reference, the amide hydrolyzed about 3.75-fold and 5.56-fold at pH 5.5 and pH 4.5, respectively, in 8 h, and more than 5-fold and 7.5-fold, respectively, after 24 h. In addition, the positive charge of $HHG2C_{18}$-L increased correspondingly with the hydrolysis of the amide (Figure 2d). The zeta potential of $HHG2C_{18}$-L gradually reached about +22 mV at pH 5.5 and +40 mV at pH 4.5 in 24 h. By comparison, $HHG2C_{18}$-L showed a zeta potential of about –20 mV at pH 7.4 even after 24 h as a consequence of the presence of carboxyl groups. These findings validated the third-stage pH response of $HHG2C_{18}$-L through a pH-cleavable linker, hexahydrobenzoic amide, which is prone to degrade in endolysosomal compartments with lower pH values, resulting in the removal of

carboxy groups from $HHG2C_{18}$, and laying a good foundation for subsequent mitochondrial targeting.

Next, to identify that charge conversion of $HHG2C_{18}$-L facilitated tumor cellular uptake, human renal carcinoma (A498) cells were incubated with C6-loaded $HHG2C_{18}$-L ($C6/HHG2C_{18}$-L) at pH 7.4 and pH 6.5 in comparison with C6-loaded SPC-L (C6/SPC-L). As shown in **Figure 3**a, the cellular uptake of $C6/HHG2C_{18}$-L at pH 6.5 was significantly higher than that at pH 7.4 ($P < 0.05$), suggesting a pH-dependent uptake process of $HHG2C_{18}$-L. In contrast, the uptake of C6/SPC-L showed no noticeable change. Moreover, that most of the uptake was due to the uptake of liposomes rather than of released C6 was confirmed by the minimal release (<1%) of C6 from the liposomes in 24 h regardless of pH value (Figure S3, Supporting

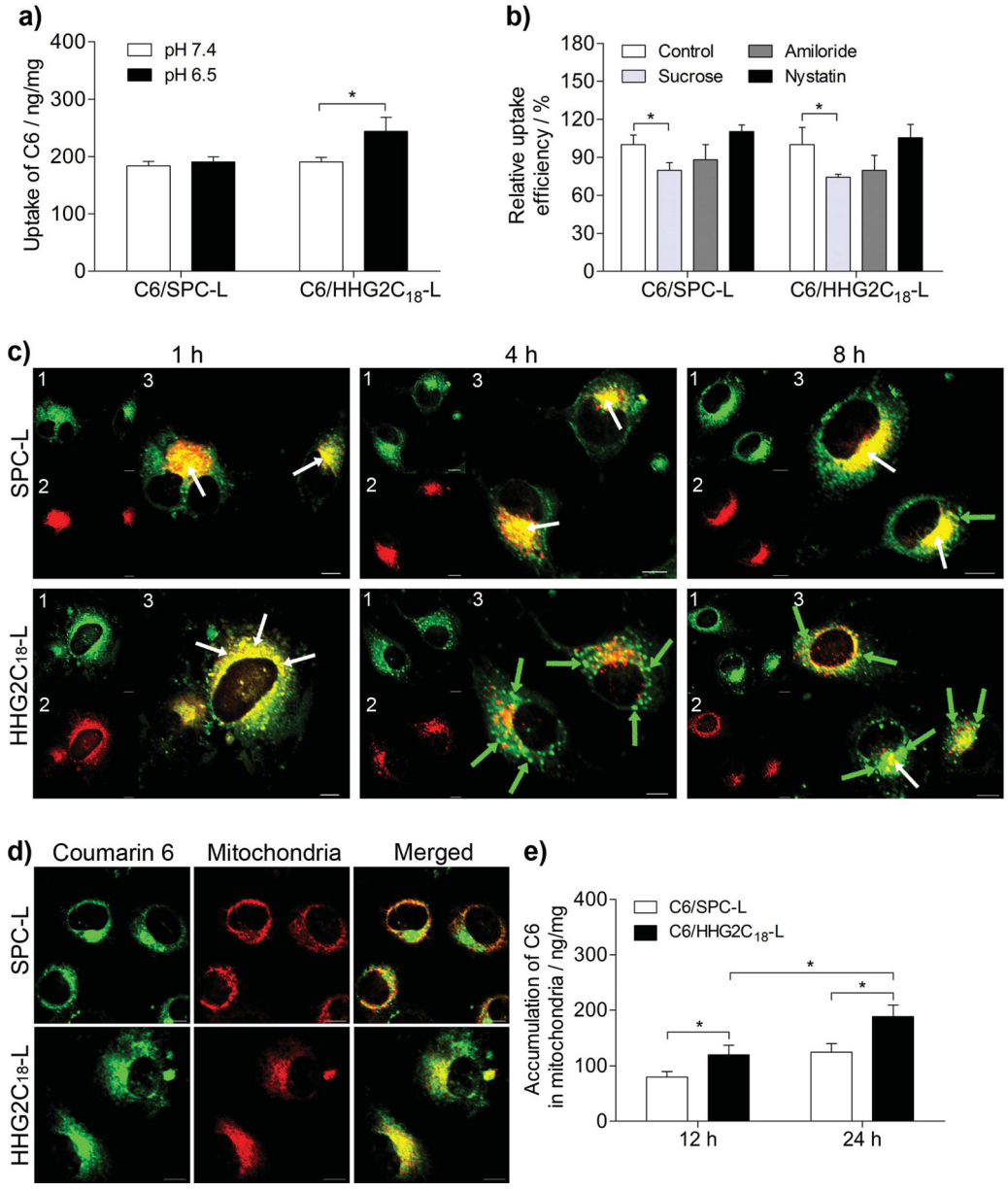

Figure 3. a) Cellular uptake of $C6/HHG2C_{18}$-L and C6/SPC-L on A498 cells at pH 7.4 and pH 6.5. Uptake of C6 is the ratio between the amount of C6 in the cells (ng) and the amount of cell proteins (mg). $^{*}P < 0.05$. b) Relative uptake efficiency of $C6/HHG2C_{18}$-L and C6/SPC-L on A498 cells in the presence of various endocytosis inhibitors. Sucrose, amiloride, and nystatin are inhibitors for clathrin-mediated endocytosis, macropinocytosis, and caveolin-mediated endocytosis, respectively. $^{*}P < 0.05$. c) Intracellular delivery of the liposomes on A498 cells at different time observed by CLSM. The late endosomes and lysosomes were stained by LysoTracker Red. 1: green-fluorescent C6; 2: red-fluorescentendolysosomes; 3: overlay of 1 and 2. White arrows indicate the occasions of coincidence between the liposomes and endolysosomes. Green arrows indicate liposomes that have escaped from endolysosomes into the cytoplasm. Scale bars are 10 μm. d) Co-localization of the liposomes into mitochondria of A498 cells at 12 h observed by CLSM. The mitochondria were stained by MitoTracker Red. Scale bars are 10 μm. e) C6 content in mitochondria isolated from A498 cells incubated with $C6/HHG2C_{18}$-L and C6/SPC-L for 12 h and 24 h. Accumulation of C6 in mitochondria is the ratio between the amount of C6 in mitochondria (ng) and the amount of mitochondrial proteins (mg). $^{*}P < 0.05$.

Adv. Mater. **2012**,
DOI: 10.1002/adma.201201498

Information). The enhanced uptake of HHG2C_{18}-L at the tumor microenvironmental pH was attributable in part to electrostatically adsorptive endocytosis. In addition, the mechanism involved in the endocytosis of C6/HHG2C_{18}-L was investigated (Figure 3b). Compared with other specific inhibitors for the corresponding endocytosis, the presence of sucrose, an inhibitor for clathrin-mediated endocytosis, significantly decreased the cellular uptake of C6/HHG2C_{18}-L ($P < 0.05$), implying that HHG2C_{18}-L as well as SPC-L encountered the primary barrier, endolysosomes, in the intracellular delivery.

In view of this, the intracellular delivery efficiency of C6/HHG2C_{18}-L on A498 cells was investigated using confocal laser scanning microscopy (CLSM). Lysosomes and mitochondria were observed as red fluorescence after the cells had been stained with specific organelle-selective dyes, while C6/HHG2C_{18}-L and C6/SPC-L were shown as green fluorescence. Co-localization of the liposomes with the specific organelle dyes appeared yellow. As shown in Figure 3c, the overwhelming majority of the green fluorescence was highly overlaid with the red fluorescence when the cells were incubated with C6/SPC-L, even after 8 h, demonstrating that it is difficult for the pH-non-responsive SPC-L to penetrate through the endolysosomes. In contrast, although C6/HHG2C_{18}-L delivered into the endolysosomes, judging from the yellow fluorescence after incubation of A498 cells with HHG2C_{18}-L for 1 h, after 4 h the green fluorescence had a significant dissociation from the red fluorescence, demonstrating the efficient endolysosomal escape of HHG2C_{18}-L. At 8 h, C6/HHG2C_{18}-L showed more effective endolysosomal release and cytoplasmic distribution, judging by the stronger green fluorescence and weaker red fluorescence. Furthermore, owing to the strong positive charge of HHG2C_{18}-L following the degradation of the hexahydrobenzoic amide, the yellow fluorescence displayed that HHG2C_{18}-L that had escaped from the endolysosomes were specifically accumulated in mitochondria in 12 h, whereas SPC-L were not mitochondriotropic, judging by the great separation between the green and red fluorescence (Figure 3d). The C6 content in the mitochondrial fraction was further quantified to quantitatively assess the role of HHG2C_{18}-L in mitochondrial targeting. As shown in Figure 3e, accumulation of C6 in mitochondria isolated from A498 cells incubated with C6/HHG2C_{18}-L was evidently higher than that incubated with C6/SPC-L ($P < 0.05$), regardless of the incubation time, and had a significant concomitant increase ($P < 0.05$) with increasing incubation time from 12 h to 24 h, which reconfirmed the observation by CLSM that HHG2C_{18}-L destroyed the endolysosomes successfully as an obstacle to cytoplasmic release and further accomplished mitochondrial targeting.

Finally, in vitro antiproliferation of CCI-779/HHG2C_{18}-L against A498 cells was evaluated at pH 7.4 and pH 6.5 using the 3-(4,5-dimethylthiazol-2-yl)-2,5-diphenyltetrazolium bromide (MTT) assay. CCI-779, a specific inhibitor of mTOR (a serine/threonine protein kinase that regulates cell growth and cell proliferation, among other things), has been previously confirmed to have a profound effect on suppressing cancer cell proliferation.[17] In addition to cytosolic mTOR, a large portion of mTOR is situated at the mitochondrial outer membrane in association with the regulation of apoptotic cell death.[18] Delivery of CCI-779 to the mitochondria is able to block mitochondrial mTOR, thereby yielding effective antiproliferative activity. As shown in

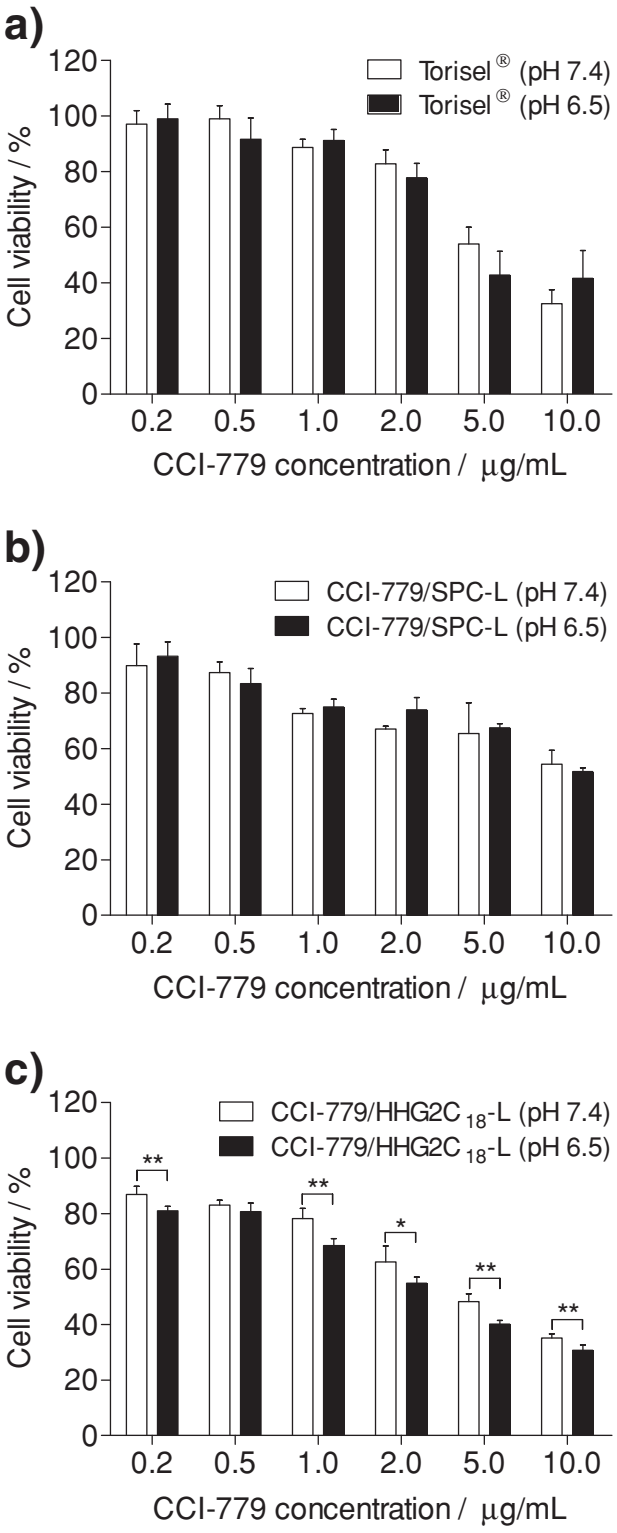

Figure 4. Antiproliferative activity of Torisel(a),CCI-779/SPC-L(b), and CCI-779/HHG2C_{18}-L (c) on A498 cells at pH 7.4 and pH 6.5 for 48 h. $^{*}P < 0.05$, $^{**}P < 0.01$.

Figure 4, CCI-779/HHG2C_{18}-L showed significantly enhanced antiproliferation at pH 6.5 relative to that at pH 7.4 ($P < 0.05$ or

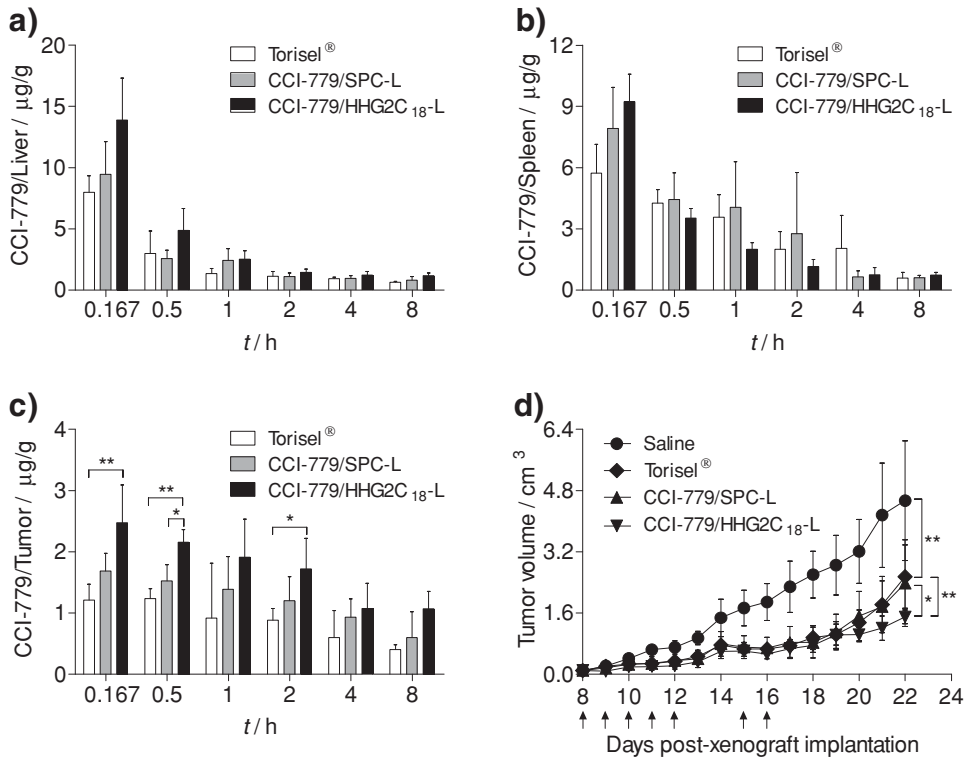

Figure 5. a–c) Biodistribution profiles of CCI-779 accumulation in the liver (a), spleen (b), and tumor (c) of Renca tumor-bearing mice after intravenous administration of different formulations of CCI-779 (10 mg kg^{-1}) at different time. CCI-779/tissue is the ratio of the amount of CCI-779 in the tissue (μg) to the weight of the tissue (g). $^{*}P < 0.05$, $^{**}P < 0.01$. d) Antitumor efficacy against Renca xenograft tumor after intravenous administration of different formulations of CCI-779 (10 mg kg^{-1}). The arrows indicate the time of intravenous administration. $^{*}P < 0.05$, $^{**}P < 0.01$.

$P < 0.01$), and even higher cytotoxicity than Torisel, the commercial formulation of CCI-779, and CCI-779-loaded SPC-L (CCI-779/SPC-L) at pH 6.5 at almost all the CCI-779 concentrations studied. The antiproliferative effects of Torisel and CCI-779/SPC-L had no noticeable improvement from pH 7.4 to pH 6.5. The bare $HHG2C_{18}$-L had no cytotoxicity under the same conditions up to a lipid concentration of 5 mg mL^{-1} (Figure S4, Supporting Information).

To verify the feasibility of $HHG2C_{18}$-L for cancer therapy in vivo, the biodistribution and antitumor efficacy of CCI-779/$HHG2C_{18}$-L were estimated in murine renal carcinoma (Renca) cell xenograft models. Just as other NPs, both CCI-779/$HHG2C_{18}$-L and CCI-779/SPC-L were subject to the phagocytosis of the reticuloendothelial system (RES), such as liver and spleen, after intravenous administration (**Figures 5**a,b). On the other hand, compared with CCI-779/SPC-L, the positive charge of CCI-779/$HHG2C_{18}$-L by charge conversion at the tumor extracellular matrix contributed to increasing the amount accumulated and prolonging the residence time of CCI-779 in the tumor tissue (Figure 5c). In addition, CCI-779/$HHG2C_{18}$-L displayed a prominent effect on tumor-size inhibition in comparison with other formulations, including saline ($P < 0.01$), Torisel ($P < 0.01$), and CCI-779/SPC-L ($P < 0.05$) (Figure 5d). No noticeable difference in tumor-size inhibition between Torisel and CCI-779/SPC-L was observed. Overall, $HHG2C_{18}$-L with multistage pH response achieved the goal of overcoming sequential physiological and biological barriers and delivering an anticancer drug efficiently.

In summary, we have developed a novel multistage pH-responsive nanocarrier for anticancer drug delivery. Charge conversion is the first-stage pH response to the mildly acidic tumor extracellular matrix. The proton sponge effect and hydrolysis of the pH-cleavable linker to increase the positive surface charge are the second- and third-stage pH responses, respectively, based on the intracellular compartmental acidity. The strengths of the smart liposomes include enhanced tumor cellular uptake, improved cytoplasmic distribution, and good mitochondrial targeting. The result provides a meaningful nanoplatform for reducing unwanted side-effects, improving the targeting efficiency and treatment efficacy, and bringing us face to face with emerging opportunities in cancer therapy.

Supporting Information

Supporting Information is available from the Wiley Online Library or from the author.

Acknowledgements

This work was supported by the National Natural Science Foundation of China (81072589), 111 Project from the Ministry of Education of China

DOI: 10.1002/adma.201201498

and the State Administration of Foreign Expert Affairs of China (No. 111-2-07), and Fundamental Research Funds for the Central Universities of China (JKY2009016).

Received: April 14, 2012
Published online:

[1] a) R. D. Hofheinz, S. U. Gnad-Vogt, U. Beyer, A. Hochhaus*Anticancer Drugs* **2005**, *16*, 691; b) M. Dell'Olio, R. P. Scalzulli, G. Sanpaolo, M. Nobile, F. S. Mantuano, A. La Sala, G. D'Arena, E. Miraglia, A. Lucania, L. Mastrullo, C. Nicola, *Leuk. Lymphoma* **2011**, *52*, 1222.

[2] a) K. S. Lee, H. C. Chung, S. A. Im, Y. H. Park, C. S. Kim, S. B. Kim, S. Y. Rha, M. Y. Lee, J. Ro, *Breast Cancer Res. Treat.* **2008**, *108*, 241; b) Y. Matsumura, K. Kataoka, *Cancer Sci.* **2009**, *100*, 572.

[3] a) W. J. Gradishar, S. Tjulandin, N. Davidson, H. Shaw, N. Desai, P. Bhar, M. Hawkins, J. O'Shaughnessy, *J. Clin. Oncol.* **2005**, *23*, 7794; b) E. Miele, G. P. Spinelli, E. Miele, F. Tomao, S. Tomao, *Int. J. Nanomedicine* **2009**, *4*, 99.

[4] a) D. Fischer, Y. Li, B. Ahlemeyer, J. Krieglstein, T. Kissel, *Biomaterials* **2003**, *24*, 1121; b) S. F. Ma, M. Nishikawa, H. Katsumi, F. Yamashita, M. Hashida, *J. Controlled Release* **2005**, *102*, 583.

[5] a) A. Muñoz Javier, O. Kreft, A. Piera Alberola, C. Kirchner, B. Zebli, A. S. Susha, E. Horn, S. Kempter, A. G. Skirtach, A. L. Rogach, J. Rädler, G. B. Sukhorukov, M. Benoit, W. J. Parak, *Small* **2006**, *2*, 394; b) Z. G. Yue, W. Wei, P. P. Lv, H. Yue, L. Y. Wang, Z. G. Su, G. H. Ma, *Biomacromolecules* **2011**, *12*, 2440; c) L. Chen, J. M. Mccrate, J. C.-M. Lee, H. Li, *Nanotechnology* **2011**, *22*, 105708.

[6] a) L. E. Gerweck, K. Seetharaman, *Cancer Res.* **1996**, *56*, 1194; b) R. A. Cardone, V. Casavola, S. J. Reshkin, *Nat. Rev. Cancer* **2005**, *5*, 786.

[7] a) H. Mok, J. W. Park, T. G. Park, *Bioconjugate Chem.* **2008**, *19*, 797; b) H. Mok, O. Veiseh, C. Fang, F. M. Kievit, F. Y. Wang, J. O. Park, M. Zhang, *Mol. Pharmaceutics* **2010**, *7*, 1930; c) J. Z. Du, T. M. Sun, W. J. Song, J. Wu, J. Wang, *Angew. Chem.Int. Ed.* **2010**, *49*, 3621; *Angew. Chem.* **2010**, *122*, 3703.

[8] a) Y. Bae, S. Fukushima, A. Harada, K. Kataoka, *Angew. Chem. Int. Ed.* **2003**, *42*, 4640; *Angew. Chem.* **2003**, *115*, 4788; b) S. Aryal, C. M. Hu, L. Zhang, *ACS Nano* **2010**, *4*, 251.

[9] a) Y. Lee, S. Fukushima, Y. Bae, S. Hiki, T. Ishii, K. Kataoka, *J. Am. Chem. Soc.* **2007**, *129*, 5362; b) Y. Lee, K. Miyata, M. Oba, T. Ishii, S. Fukushima, M. Han, H. Koyama, N. Nishiyama, K. Kataoka, *Angew. Chem. Int. Ed.* **2008**, *47*, 5163; *Angew. Chem.* **2008**, *120*, 5241.

[10] a) C. Y. Lai, C. M. Wiethoff, V. A. Kickhoefer, L. H. Rome, G. R. Nemerow, *ACS Nano* **2009**, *3*, 691; b) C. V. Kelly, M. G. Liroff, L. D. Triplett, P. R. Leroueil, D. G. Mullen, J. M. Wallace, S. Meshinchi, J. R. Baker, B. G. Orr, M. M. Banaszak Holl, *ACS Nano* **2009**, *3*, 1886; c) Y. Obata, S. Tajima, S. Takeoka, *J. Controlled Release* **2010**, *142*, 267.

[11] a) E. S. Lee, D. Kim, Y. S. Youn, K. T. Oh, Y. H. Bae, *Angew. Chem.* **2008**, *120*, 2452; *Angew. Chem. Int. Ed.* **2008**, *47*, 2418; b) C. J. Ke, T. Y. Su, H. L. Chen, H. L. Chiang, P. C. Chu, Y. Xia, H. W. Sung, *Angew. Chem.* **2011**, *123*, 8236; *Angew. Chem. Int. Ed.* **2011**, *50*, 8086.

[12] a) J. You, D. T. Auguste, *Nano Lett.* **2009**, *9*, 4467; b) Z. X. Zhou, Y. Q. Shen, J. B. Tang, M. H. Fan, E. A. Van Kirk, W. J. Murdoch, M. Radosz, *Adv. Funct. Mater.* **2009**, *19*, 3580; c) H. Yu, Y. Zou, Y. Wang, X. Huang, G. Huang, B. D. Sumer, D. A. Boothman, J. Gao, *ACS Nano* **2011**, *5*, 9246.

[13] S. Fulda, L. Galluzzi, G. Kroemer, *Nat. Rev. Drug Discovery* **2010**, *9*, 447.

[14] V. Gogvadze, S. Orrenlus, B. Zhivotovsky, *Trends Cell Biol.* **2008**, *18*, 165.

[15] V. Weissig, V. P. Torchilin, *Adv. Drug Delivery Rev.* **2001**, *49*, 127.

[16] a) J. J. Morris, M. I. Page, *J. Chem. Soc. Chem. Commun.* **1978**, 591; b) P. Xu, E. A. Van Kirk, Y. Zhan, W. J. Murdoch, M. Radosz, Y. Shen, *Angew. Chem. Int. Ed.* **2007**, *46*, 4999; *Angew. Chem.* **2007**, *119*, 5087.

[17] a) I. M. Ghobrial, T. E. Witzig, A. A. Adjei, *CA: Cancer J. Clinicians* **2005**, *55*, 178; b) S. Vignot, S. Faivre, D. Aguirre, E. Raymond, *Ann. Oncol.* **2005**, *16*, 525.

[18] a) B. N. Desai, B. R. Myers, S. L. Schreiber, *Proc. Natl. Acad. Sci. USA* **2002**, *99*, 4319; b) A. Ramanathan, S. L. Schreiber, *Proc. Natl. Acad. Sci. USA* **2009**, *106*, 22229.